AGU PUBLICATIONS

Geophysical Research Letters

RESEARCH LETTER
10.1002/2017GL075922

Key Points:
- SIF captures seasonal GPP dynamics better than EVI and PRI, especially for evergreen forest sites
- SIF is more sensitive than EVI and PRI to site-level interannual GPP variability across all southwestern North America ecoregions
- Incorporation of SIF could significantly improve satellite-based GPP estimates for dryland ecosystems

Supporting Information:
- Supporting Information S1

Correspondence to:
W. K. Smith,
wksmith@email.arizona.edu

Citation:
Smith, W. K., Biederman, J. A., Scott, R. L., Moore, D. J. P., He, M., Kimball, J. S., … Litvak, M. E. (2018). Chlorophyll fluorescence better captures seasonal and interannual gross primary productivity dynamics across dryland ecosystems of southwestern North America. *Geophysical Research Letters*, *45*, 748–757. https://doi.org/10.1002/2017GL075922

Received 3 OCT 2017
Accepted 29 DEC 2017
Accepted article online 4 JAN 2018
Published online 19 JAN 2018

Chlorophyll Fluorescence Better Captures Seasonal and Interannual Gross Primary Productivity Dynamics Across Dryland Ecosystems of Southwestern North America

W. K. Smith[1], J. A. Biederman[2], R. L. Scott[2], D. J. P. Moore[1], M. He[3], J. S. Kimball[3], D. Yan[1], A. Hudson[1], M. L. Barnes[1], N. MacBean[1], A. M. Fox[1], and M. E. Litvak[4]

[1]School of Natural Resources and the Environment, University of Arizona, Tucson, AZ, USA, [2]Southwest Watershed Research Center, USDA Agricultural Research Service, Tucson, AZ, USA, [3]Numerical Terradynamic Simulation Group, College of Forestry and Conservation, University of Montana, Missoula, MT, USA, [4]Department of Biology, University of New Mexico, Albuquerque, NM, USA

Abstract Satellite remote sensing provides unmatched spatiotemporal information on vegetation gross primary productivity (GPP). Yet understanding of the relationship between GPP and remote sensing observations and how it changes with factors such as scale, biophysical constraint, and vegetation type remains limited. This knowledge gap is especially apparent for dryland ecosystems, which have characteristic high spatiotemporal variability and are under-represented by long-term field measurements. Here we utilize an eddy covariance (EC) data synthesis for southwestern North America in an assessment of how accurately satellite-derived vegetation proxies capture seasonal to interannual GPP dynamics across dryland gradients. We evaluate the enhanced vegetation index, solar-induced fluorescence (SIF), and the photochemical reflectivity index. We find evidence that SIF is more accurately capturing seasonal GPP dynamics particularly for evergreen-dominated EC sites and more accurately estimating the full magnitude of interannual GPP dynamics for all dryland EC sites. These results suggest that incorporation of SIF could significantly improve satellite-based GPP estimates.

1. Introduction

Year-to-year variability of the atmospheric CO_2 growth rate is primarily driven by fluctuations in carbon uptake by land ecosystems (Keeling et al., 1995). Arid and semiarid dryland ecosystems cover ~40% of the global land surface, and mounting evidence suggests that they play a dominant role in driving the interannual variability of CO_2 uptake by terrestrial ecosystems (Ahlström et al., 2015; Jung et al., 2017; Poulter et al., 2014). Drylands are characterized by frequent drought and high temperatures and thus are also excellent study systems for improved understanding of coupled drought–vegetation dynamics (Scott et al., 2015). Yet there is a relative paucity of continuous, long-term measurements of dryland vegetation dynamics, resulting in dryland gross primary productivity (GPP) estimates that are poorly constrained by observational data including estimates from remote sensing, atmospheric inversion models, empirical regression models, and terrestrial biosphere models (Biederman et al., 2017; Jung et al., 2011; Ma et al., 2015; Verma et al., 2014; Xiao et al., 2014). Improved understanding of dryland GPP dynamics is a critical step toward accurate prediction and forecasting of interannual variability of terrestrial CO_2 uptake and, in turn, atmospheric CO_2 concentrations.

Satellite remote sensing is unmatched in spatiotemporal coverage and has been used to quantify global GPP dynamics since the early 1980s (Coops et al., 2010; Monteith, 1972; Potter et al., 1993; Running et al., 2004; Smith et al., 2016). Satellite-based GPP estimates have helped shape our current understanding of dryland function within the context of the broader Earth system (Ahlström et al., 2015; Jung et al., 2017; Poulter et al., 2014). However, GPP cannot be directly observed, and satellite-derived GPP estimates rely heavily on vegetation indices (VIs) such as the normalized difference vegetation index (NDVI) and enhanced vegetation index (EVI) that provide information on vegetation state (e.g., photosynthetic capacity), not physiological function (e.g., photosynthetic activity). Operational GPP products based on this approach are widely used and available since the early 2000s as NASA Moderate Resolution Imaging Spectroradiometer (MODIS) products (Running et al., 2004; Zhao et al., 2005; Zhao & Running, 2010), and more recently as NASA Soil

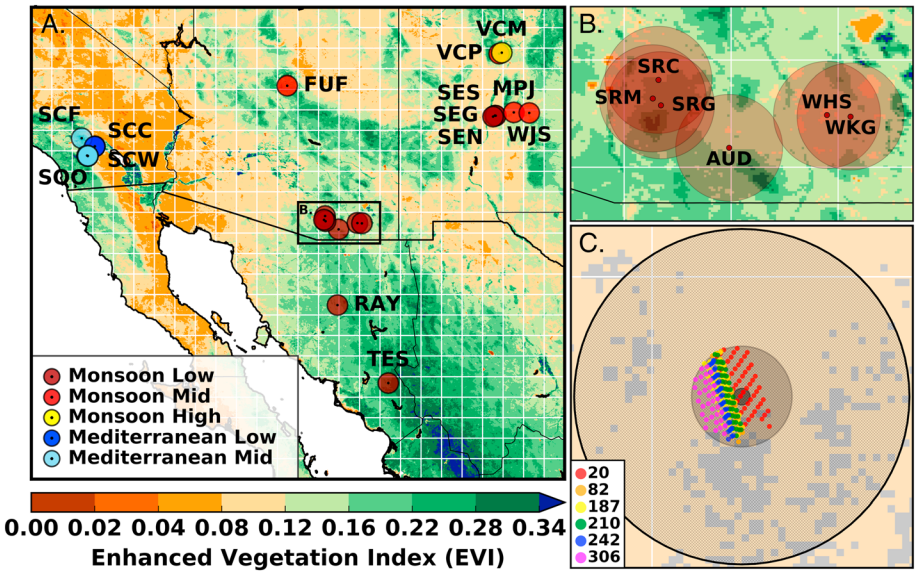

Figure 1. Multiscale maps of the Southwest EC flux tower network. (a) View of the EC sites used in the analysis with regional mean MODIS EVI. (b) View of the cluster of flux tower sites in southeast Arizona. (c) View of the Santa Rita Mesquite (SRM) flux tower site within the southeast Arizona cluster. The white gridlines correspond to the pixels of SIF_{GOME2}. The EC site marker colors in Figures 1a and 1b indicate subregional groupings of sites sharing similar seasonal climatic and ecological dynamics. Innermost and outermost circles around each flux tower site indicate the 3 km fine-resolution and 0.5° coarse-resolution EC footprints analyzed in this study. The colored points in Figure 1c correspond to the day of year of available SIF_{OCO2} observations for the year 2016, whereas the underlying tan color indicates areas classified as shrubland. For site codes and descriptions, see Table S1.

Moisture Active Passive products (Jones et al., 2017). Although the spatial variability in satellite-derived GPP is generally consistent with field measurements (Biederman et al., 2017; Verma et al., 2014), satellite-derived GPP suffers from substantial uncertainties at seasonal to interannual timescales, particularly for dryland ecosystems. For example, across the drylands of southwestern North America, the MODIS GPP product was found to only account for 20–30% of the interannual variation in eddy covariance flux-based GPP observations (Biederman et al., 2017). The relative poor performance of remote sensing-based GPP estimates across drylands is likely due to the high heterogeneity of dryland ecosystems as well as limitations of greenness-based VIs (Biederman et al., 2017; Verma et al., 2014).

By potentially providing information directly related to vegetation physiological function, emerging solar-induced fluorescence (SIF) and photochemical reflectivity index (PRI) data offer a significant advancement over traditional VIs (Frankenberg et al., 2011; Penuelas et al., 2011; Schimel et al., 2015; Sun et al., 2017; Vicca et al., 2016). Vegetation fluorescence is the light reemitted from chlorophyll during photosynthesis and thus represents a potential direct proxy for photosynthetic activity (Manish Verma et al., 2017; Parazoo et al., 2014; Schimel et al., 2015; Sun et al., 2017; Wood et al., 2016; Zhang et al., 2014). Fluorescence has been measured for decades at the leaf level using the pulse amplitude-modulation technique and is now also being measured passively (i.e., SIF) from remote sensing platforms (Porcar-Castell et al., 2014). Alternatively, PRI detects nonphotochemical quenching via changes in the foliar carotenoid pigment pool and thus dynamically tracks changes in photosynthetic activity (Gamon et al., 2016; Porcar-Castell et al., 2014). PRI has been used as a photosynthesis proxy over a range of climate conditions and vegetation types (Gamon et al., 2016; Gamon, Peñuelas, & Field, 1992; He et al., 2016). While previous analyses have explored these emerging proxies in tropical (Lee et al., 2013), temperate (Yang et al., 2015), boreal (Walther et al., 2016), grassland (Jeong et al., 2017), and cropland ecosystems (Wood et al., 2016), their ability to capture GPP dynamics across heterogeneous dryland ecosystems remains relatively unknown.

Here we address this knowledge gap by evaluating the ability of current satellite-based EVI, SIF, and PRI data sets to detect seasonal to interannual changes in GPP across a new synthesis of data from eddy covariance (EC) flux tower sites distributed across southwestern North America (Figure 1). These sites cover wide ranges

in annual precipitation (200–1,000 mm) and annual temperatures (2–25°C) and thus represent key climatically distinct subregions within the fairly broad dryland classification (Biederman et al., 2016, 2017). These newly synthesized observational data enable a robust benchmark to test the potential of SIF and PRI as next-generation GPP proxies that are more closely linked to plant physiological function.

2. Data and Methods

2.1. Study Region and Sites

The study region (hereafter referred to as "the Southwest") includes EC sites in Arizona, New Mexico, and portions of southern California within the conterminous USA, and sites in Sonora, Mexico (Figure 1). The Southwest is generally characterized by water limitation at the annual scale and has large spatial gradients in mean annual precipitation and temperature due to interactions among topography, latitude, weather patterns, and distance from oceans (Biederman et al., 2017). We used 20 EC flux sites distributed across the major climatic and ecological subregions of the Southwest including Monsoon Low, Mid, and High elevation, and Mediterranean Low and Mid elevation sites (Figure 1 and Table S1 in the supporting information). We included in the analysis all available EC sites with a minimum of three observation years (total site years = 118 years) during the study period from 2007 to 2016; the resulting site years selected for this analysis are summarized in Table S1. The dominant International Geosphere-Biosphere Programme (IGBP) vegetation classes of the region include grassland, open and closed shrubland, savanna and woody savanna, mixed forest, and evergreen needleleaf forest (Table S1). For additional site details, see Table S1 and https://www.fluxdata.org/.

2.2. Satellite Data

We used EVI data derived from the MODIS (Moderate Resolution Imaging Spectroradiometer) sensor onboard the NASA EOS Terra satellite from 2000 to 2016. We used the 16 day composite 1 km resolution MODIS/Terra EVI (MOD13A2 V006) data product. The 16 day pixel reliability data layer that accompanied the EVI data was used to identify and remove lower quality data.

We used PRI data derived from the MODIS spectral reflectance records obtained from the NASA EOS Terra and Aqua satellites from 2000 to 2016. We used daily 1 km resolution PRI derived from the Terra/Aqua MODIS Level 1B reflectance (MOD/MYD021KM) data product. MODIS PRI uses a broad range of wavelengths that generally track changes in foliar chlorophyll and carotenoid pigment levels (Gamon et al., 2016). We derived PRI using MODIS Band 11 (526–536 nm) and Band 13 (662–672 nm) reflectance data following the methods of He et al. (2016). Low-quality reflectance data were filtered using the daily 1 km resolution Terra/Aqua MODIS Cloud product (MOD/MYD35_L2). Please see He et al. (2016) for more detail on the PRI derivation.

We used SIF data derived from the GOME-2 (Global Ozone Mapping Experiment) sensor onboard the European Organisation for the Exploitation of Meteorological Satellites MetOp satellites from 2007 to 2016 (hereafter, SIF_{GOME2}). Specifically, we used the monthly composite, 0.5° resolution GOME-2/MetOp-A Version 2.6 SIF data product. These data are based on channel 4 of the GOME-2 sensor with ~0.5 nm spectral resolution and wavelengths between 734 and 758 nm. The GOME-2 sensor experienced significant degradation over its lifetime, particularly in the early part of the record. To account for this, the SIF_{GOME2} data product was corrected by adjustments based on the degradation of solar irradiance values (Joiner et al., 2016). We further checked for SIF_{GOME2} degradation across EC sites by analyzing long-term trends in the time series data (Figure S1). We found that across EC sites, SIF_{GOME2} seasonal and interannual variability was much larger than the mean long-term trend (Figure S1). Please see Joiner et al. (2013) and Joiner et al. (2016) for more detail on the SIF_{GOME2} data.

We also used SIF data derived from the NASA OCO-2 (Orbiting Carbon Observatory) satellite from 2015 to 2016 (hereafter SIF_{OCO2}). While OCO-2 collects spatially dense samples at relatively high spatial resolution (1.3 by 2.5 km), the global coverage on a monthly time step is relatively sparse due to a relatively narrow instrument observation swath (Verma et al., 2017). We combined SIF_{OCO2} signals at 757 nm and 771 nm by applying a standard signal strength correction factor of 1.4 to the weaker 771 nm signal (Verma et al., 2017; Wood et al., 2016). SIF_{OCO2} data were provided with accompanying ancillary data including data quality

and daily correction factors, which were used to remove low-quality data and convert instantaneous SIF_{OCO2} to daily average SIF_{OCO2} values, respectively.

2.3. Space and Time Scaling

For each EC site, data were spatially aggregated based on (i) a 3 km fine-resolution and (ii) a 0.5° coarse-resolution site footprint in order to control for the different native resolutions of the utilized satellite data sets described above. The fine-resolution footprint was defined as a 3 km diameter circle around each EC site location, while the coarse-resolution footprint was defined as a 0.5° diameter circle around each EC site (Figure 1). For each data product, all pixels with a centroid that fell within the footprint were averaged.

Due to the coarse resolution of SIF_{GOME2} data, we did not extract a 3 km fine-resolution time series for these data. Instead, we estimated a fine-resolution SIF_{OCO2} time series for selected sites (SRM and VCP only). We aggregated all SIF_{OCO2} observations that had a measurement centroid falling within a 0.25° diameter circle surrounding the tower site. We further filtered SIF_{OCO2} observations to include only those with a similar land cover type to that of the dominant land cover type of the 3 km footprint (Figure 1 and Table S1).

To help explain differences due to spatial scaling, we assessed differences in vegetation land cover types between the fine- versus coarse-resolution footprints across tower sites. We quantified each site by its dominant (>10% cover) land cover type at both the 3 km fine and 0.5° coarse-resolution footprints using MODIS (MCD12Q1 V005) land cover data and International Geosphere-Biosphere Programme (IGBP) classification (Table S1).

SIF_{GOME2} and SIF_{OCO2} use a simple cosine correction based on the solar zenith angle to temporally scale from instantaneous to daily integrated values. This simple method of temporal scaling thus assumes diurnal symmetry in SIF dynamics. We carried out an assessment of GPP dynamics at hourly timescales for the SRM site—the most arid savanna EC sites in our synthesis where we expected the greatest diurnal GPP asymmetry—to evaluate the validity of the SIF scaling approach in capturing daily GPP dynamics (Figure S2). While diurnal asymmetry was apparent in hourly GPP estimates, we found that controlling for the overpass times of GOME-2 (9:00–10:00 LT) and OCO-2 (13:00–14:00 LT) resulted in very similar seasonal GPP dynamics (r = 0.998 and r = 0.984, respectively; Figure S2). These results suggest that for the purposes of our study, scaling instantaneous to daily integrated SIF using cosine correction is appropriate for capturing seasonal dynamics.

2.4. Data Analysis

For the seasonal analysis, all data were aggregated to monthly mean values (n = 12). To compare relative seasonal variations in satellite proxies and EC GPP, all data sets were normalized to range from 0 to 1. Linear regression analysis was performed at the individual EC site and subregional scale (Table S2). For the interannual analysis, monthly data were summed annually for each year of observation. For each site, only site-years with a corresponding complete monthly record were used. To compare relative interannual variations in the satellite proxies and EC GPP, data were converted to Z-scores, which represent variations in terms of standard deviations from the mean. Linear regressions were preformed to evaluate relative differences in the ability of the satellite proxies to capture the full range of interannual variability in EC GPP estimates (Table S3). Thus, temporal slopes were interpreted such that values greater than 1 represent oversensitivity, whereas values less than 1 represent undersensitivity to interannual EC GPP variations (Biederman et al., 2017). Temporal regressions were only performed on long-term EC sites with data records longer than 4 years. Relationships were evaluated based on the correlation coefficient (r), root-mean-square error, bias, slope, and p value of the regression fit using the "lm" function of the "stats" package of the open source R programming language.

3. Results

3.1. Seasonal GPP Dynamics

SIF_{GOME2} was found to most consistently capture seasonal GPP dynamics (r = 0.91) compared to EVI (r = 0.83) and PRI (r = 0.78) across the Southwest eddy covariance sites examined (Figure 2 and Table S2). SIF_{GOME2} captured seasonal GPP dynamics better across Monsoon Low, Monsoon Mid, and Mediterranean Mid subregions (Figure 2 and Table S2). Conversely, EVI was slightly better at capturing seasonal GPP dynamics

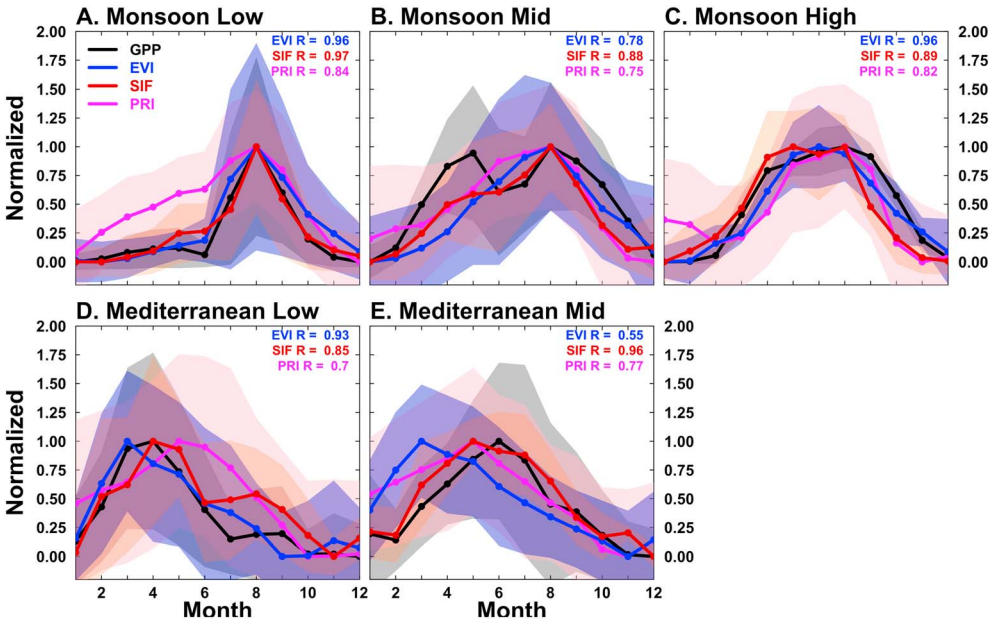

Figure 2. Mean monthly (±1 standard deviation) GPP, EVI, SIF_{GOME2}, and PRI based on a 0.5° coarse-resolution site footprint. (a–e) Subregional aggregations of EC sites based on similarity in seasonal climatic and ecological dynamic. Site-level and subregional-level statistics can be found in Table S2.

across Mediterranean Low and Monsoon High subregions (Figure 2 and Table S2). Comparison of the 0.5° coarse and 3 km fine-resolution site footprints for EVI and PRI revealed that these findings are largely robust across spatial scales, with the exception of the Mediterranean Mid subregion (Figures S3 and S4).

Monsoon Mid sites included two evergreen forest sites (FUF and VCP) and two evergreen woodland sites (MPJ and WJS) at 1,900 to 2,500 m elevation (Table S1). GPP at these sites typically declines with snowmelt-derived soil moisture during early summer and then resumes with the arrival of monsoon precipitation in July–August, resulting in a characteristic bimodal GPP seasonality (Biederman et al., 2017). SIF_{GOME2} captures both the spring and summer peaks in GPP seasonality, while EVI and PRI capture only a single seasonal peak resulting from the summer monsoon precipitation (Figure 2). While there is some variation across these sites, we show that this general pattern of SIF sensitivity to early season GPP dynamics is observable across individual EC sites within the subregion (Figure S5). We found further evidence that SIF better captures early-season GPP dynamics by evaluating SIF_{OCO2} retrievals for the Valles Caldera evergreen forest site (VCP) in New Mexico (Figure S6). We found that both SIF_{GOME2} and SIF_{OCO2} captured significant early-season photosynthetic activity consistent with GPP patterns, whereas EVI and PRI did not capture early-season photosynthetic activity (Figure S6).

Mediterranean Mid subregions included two sites comprising one oak-pine forest (SCF) and one chamise chaparral (SOB) site at 1,500 to 1,700 m elevation (Table S1). GPP at these sites typically peaks in May and is sustained through the summer months given sufficient winter soil moisture stores and/or summer rainfall (Biederman et al., 2017). SIF_{GOME2} and PRI were found to accurately capture peak GPP (Figure 2 and Table S2), whereas EVI peaked relatively earlier in the season (Figure 2).

The Monsoon High subregion included only one evergreen forest site (VCM) at ~3,000 m elevation (Table S1). Seasonal GPP at this site is typically sustained by snowmelt from roughly May to June, and monsoon precipitation from roughly July to August, resulting in a single GPP peak (Biederman et al., 2017). EVI and SIF_{GOME2} both captured these single peaks in GPP (Figure 2 and Table S2).

The Monsoon Low subregion included desert grassland (AUD, SEG, SRG, and WKG), shrubland (RAY, SES, SRC, and WHS), and savanna (SRM and TES) at 500 to 1,600 m elevation (Table S1). Seasonal GPP at these sites is dominated by a single late summer peak driven by monsoonal precipitation (Biederman et al., 2017). EVI, SIF_{GOME2}, and PRI all captured these single peaks in GPP (Figure 2 and Table S2).

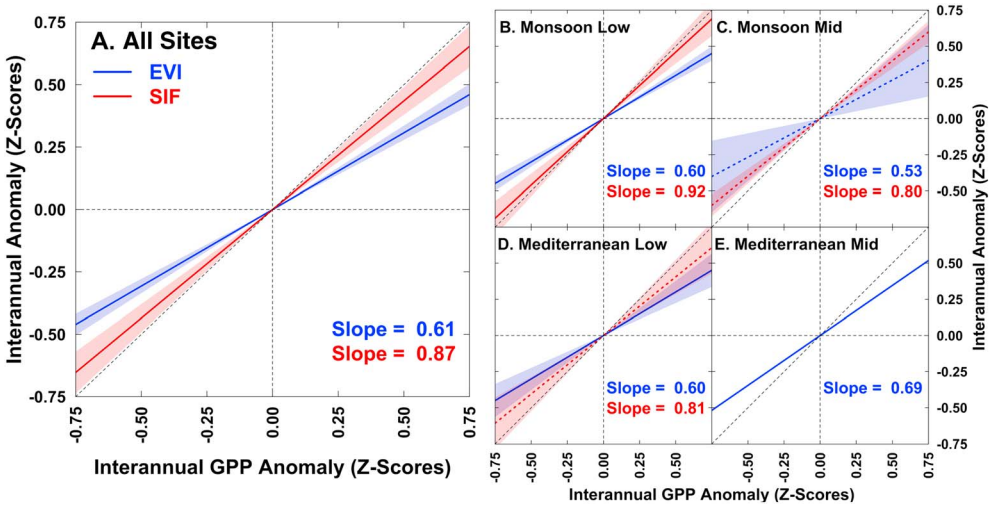

Figure 3. Linear fit (±SD) between the interannual variability of GPP and EVI, SIF_{GOME2}, and PRI based on a 0.5° coarse-resolution site footprint. (a) Linear fit through annual anomalies from all sites. (b–d) Linear fit for all annual anomalies for a given subregion. The solid lines indicate a linear fit significant at the 0.05 significance level, whereas the dashed lines indicate a linear fit significant at the 0.125 significance level. Linear fits with an associated significance level greater than 0.125 are not shown. PRI not included due to significance level greater than 0.125 across all subregions. Monsoon High subregion not included due to limited site years. The dashed black lines show the axis origins as well as the ideal 1:1 relationship. Site-level statistics can be found in Table S3.

The Mediterranean Low subregion included one evergreen pinyon-juniper (SCW) and one chaparral (SCC) site at ~1,300 m elevation (Table S1). Seasonal GPP at these sites typically peaks in the early spring (March–April), followed by an early summer dry-down (Biederman et al., 2017). A second smaller GPP peak sometimes occurs in the summer months, depending on summer precipitation (Biederman et al., 2017). EVI, SIF_{GOME2}, and PRI were found to capture the early season peak in GPP. Notably, SIF_{GOME2} appears to better capture the late season smaller peak in GPP (Figure 2).

3.2. Interannual GPP Dynamics

SIF_{GOME2} was found to most consistently capture the within-site slope of interannual GPP observations (temporal slope = 0.87, $p < 0.001$), indicating that SIF better captures interannual variability in GPP (Figure 3). By contrast, EVI (temporal slope = 0.61, $p < 0.001$) and PRI (temporal slope = 0.20, $p = 0.44$) showed relatively reduced sensitivity to interannual variability in GPP (Figure 3 and Table S3). We observed these trends across all subregions of the Southwest, although trends in the Monsoon High and Mediterranean Mid subregions were nonsignificant due largely to the limited number of observation years (Figure 3 and Table S3). Surprisingly, utilizing the 3 km fine-resolution site footprint significantly decreased the sensitivity of EVI to GPP interannual variability (slope = 0.38; $p < 0.05$) (Figure S7).

We evaluated the 2016 GPP anomaly at the SRM savanna site to further explore differences in interannual GPP sensitivities (Figure 4). In 2016, due to the previous year's above average precipitation, SRM GPP increased by 63% relative to the decadal mean (2007–2016) (Figure 4). Both SIF_{GOME2} and SIF_{OCO2} observations were able to roughly capture the pattern and magnitude of the 2016 GPP anomaly. In contrast, EVI and PRI were largely insensitive to the 2016 GPP anomaly. Notably, both EVI and PRI appear to miss the large increase in springtime GPP that is a defining feature of the 2016 GPP anomaly. Utilizing the 3 km fine-resolution site footprint did not improve the interannual sensitivity of EVI or PRI (Figure 4).

4. Discussion

4.1. Seasonal GPP Dynamics

We found that SIF_{GOME2} is an improved proxy for seasonal GPP dynamics relative to EVI and PRI for the Southwest (Figure 2 and Table S2). SIF_{GOME2} showed the best performance of the three proxies examined for sites within the Monsoon and Mediterranean Mid subregions—subregions at relatively higher

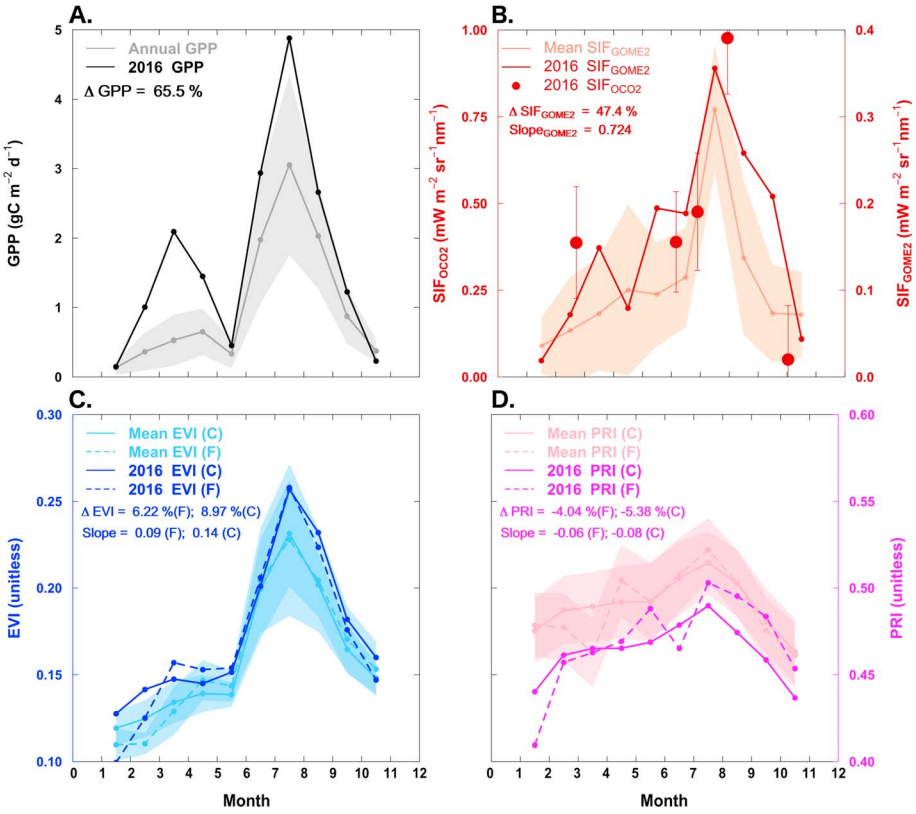

Figure 4. The 2016 anomaly for the Santa Rita Experimental Range Mesquite (SRM) EC flux tower site. Monthly (a) GPP, (b) EVI, (c) SIF_{GOME2} and SIF_{OCO2}, and (d) PRI. Reported on each plot are the integrated annual change (Δ) and the linear temporal slope (slope) between a given satellite index and GPP for both the 30 min coarse (C) and 3 km fine (F)-resolution site footprints. See Figure 1c for a map of the SRM site and SIF_{OCO2} observations.

elevations and with higher proportions of evergreen forests and woodlands (Table S1). For these sites, SIF_{GOME2} was able to capture early-season photosynthesis that was not captured by either EVI or PRI (Figure S5 and Table S2). A likely explanation for this result is that proxies based on changes in vegetation greenness (i.e., EVI and PRI) fail to capture seasonal photosynthetic activity of evergreen trees, since greenness and photosynthesis are often decoupled for this vegetation type (Verma et al., 2014; Vicca et al., 2016; Walther et al., 2016), whereas SIF is a direct measure of photosynthetic activity (Manish Verma et al., 2017; Walther et al., 2016; Yang et al., 2017). We suspect that EVI and PRI seasonality in these subregions is more likely tracking changes in greenness of intermixed (e.g., subcanopy) annual and deciduous vegetation (Manish Verma et al., 2017; Verma et al., 2014; Vicca et al., 2016). This finding is supported by the 2016 GPP anomaly at the VCP site, for which both SIF_{GOME2} and SIF_{OCO2} time series were found to capture early season photosynthetic activity, whereas EVI and PRI did not (Figure S6). Our results are consistent with previous studies that have demonstrated similar potential for SIF as an improved GPP proxy (Manish Verma et al., 2017; Perez-Priego et al., 2015; Sanders et al., 2016; Wood et al., 2016; Yang et al., 2017; Zarco-Tejada et al., 2016; Zhang et al., 2014), although few to our knowledge have evaluated dryland, water-limited ecosystems such as these.

SIF_{GOME2} was well correlated with seasonal GPP for Monsoon and Mediterranean Low sites, but to a roughly equal or slightly lesser degree than EVI (Figure 2 and Table S2). EVI is likely an equally useful GPP proxy for low-elevation sites since they are dominated by ephemerally green vegetation (dryland shrubs and grasses) that "green up" and "brown down" in synchronization with seasonal GPP dynamics (Biederman et al., 2017; Ma et al., 2014; Manish Verma et al., 2017; Verma et al., 2014). SIF_{GOME2} captured these seasonal GPP dynamics as well, but likely suffered from a relatively low signal-to-noise ratio (Joiner et al., 2013, 2016). PRI was also correlated with seasonal GPP for these sites, yet with consistently lowest correlation

coefficients across subregions. This is likely due to the relatively low reflectance ratio of the data input MODIS Band 13, which causes substantial information loss over high-reflectance deserts and sparsely vegetated ecosystems of the Southwest (He et al., 2016). The limitations associated with SIF_{GOME2} and PRI data highlight the need for more field-level studies for which spatiotemporal resolution and the signal-to-noise ratio can be improved, thus enabling a more complete and unbiased evaluation of the information contained in these indices.

4.2. Interannual GPP Dynamics

We found that SIF_{GOME2} is more sensitive to interannual GPP variability relative to EVI and PRI for the Southwest (Figure 3 and Table S3). This is likely due to increased sensitivity of SIF to GPP during periods of water stress (Perez-Priego et al., 2015; Walther et al., 2016), as well as to a lesser extent relative insensitivity of SIF to background soil reflectance (Badgley et al., 2017). Increased SIF sensitivity to interannual variability of GPP was surprisingly consistent across subregions of the Southwest, whereas EVI and PRI were both found to have notably lower sensitivity to interannual variability of GPP (Figures 3 and S7). Interestingly, interannual sensitivity of EVI was further reduced when analyzing a 3 km fine-resolution site footprint (Figure S7). We posit again that the inclusion of more ephemerally green vegetation that "green up" and "brown down" in synchronization with GPP dynamics when using the 0.5° coarse-resolution site footprint may have resulted in relatively higher apparent EVI and PRI interannual sensitivity (Sims et al., 2014).

We further evaluated the 2016 GPP anomaly at the SRM EC site (Figure 4). We note that while the IGBP land cover class for this site is shrub-dominated, the site is more accurately classed as a savanna ecosystem due to an equal proportion of intermixed mesquite trees and understory shrubs and grasses (Scott et al., 2009). In 2016, SRM had the highest GPP for the 13-year site record due to continuous years of above average precipitation. SIF_{GOME2} and SIF_{OCO2} captured seasonal dynamics and an overall magnitude increase comparable to that of the EC GPP patterns, whereas EVI and PRI appeared relatively insensitive to the 2016 GPP anomaly, particularly in the early spring (Figure 4). We interpret this finding as further evidence that among the vegetation indices evaluated here, SIF is most sensitive to interannual GPP variability since it is more directly detecting actual changes in photosynthetic activity of both the mesquite trees and grasses, whereas EVI may miss changes of photosynthetic activity, particularly for mesquite vegetation, which dominate the early spring GPP signal (Scott et al., 2009).

5. Conclusions

Our findings show that satellite-based SIF could enhance our ability to capture both seasonal and interannual GPP dynamics across dryland ecosystems. SIF appears to better capture seasonal periods of water stress and early season GPP dynamics, particularly for evergreen forest sites. In addition, SIF appears to more accurately capture the relative range of interannual variations in GPP across dryland gradients. Currently, most satellite-based GPP estimates are derived from VI-based proxies (Ma et al., 2016; Sims et al., 2008; Smith et al., 2016). Insights presented here suggest that SIF-based GPP estimates could contribute to improved understanding of drylands and their role in driving interannual variability of the atmospheric CO_2 growth rate (Biederman et al., 2017). The limited spatiotemporal resolution of currently available satellite-based SIF observations remains a key challenge in our ability to fully evaluate the SIF-GPP relationship. Data downscaling (Duveiller & Cescatti, 2016) and data assimilation (Lee et al., 2015) are promising approaches for dealing with this challenge and should remain areas of research priority. Upcoming satellite missions including ESA TROPOMI (Guanter et al., 2015) and NASA OCO-3 (Stavros et al., 2017) will continue to revolutionize satellite-based monitoring of SIF.

Acknowledgments
Funding for the AmeriFlux core sites used in this paper was provided by the DOE's Office of Science. Additional support was provided by NASA (NNH16ZDA001N), USDA cooperative agreements (58-0111-17-013), and DOE's Regional and Global Climate Modeling Program (DE-SC0016011). EC GPP data used here are available through the Ameriflux data archive or by contacting individual site PIs directly (http://ameriflux.lbl.gov). The EVI data used here are available via the NASA Land Processes Distributed Active Archive Center (https://lpdaac.usgs.gov/dataset_discovery/modis/). The PRI data used here are available via the Level-1 and Atmosphere Archive and Distribution System Distributed Active Archive Center (LAADS DAAC; https://ladsweb.modaps.eosdis.nasa.gov/about/purpose/). The SIF_{GOME2} used here are available via the Aura Validation Data Center (AVDC; https://avdc.gsfc.nasa.gov/). The SIF_{OCO2} data used here are available via the JPL OCO-2 Data Center (https://oco.jpl.nasa.gov/). Code used for analyses and figures have been archived in a GitHub repository (https://github.com/wkolby/).

References

Ahlström, A., Raupach, M. R., Schurgers, G., Smith, B., Arneth, A., Jung, M., … Zeng, N. (2015). The dominant role of semi-arid ecosystems in the trend and variability of the land CO_2 sink. *Science*, *348*(6237), 895–899. https://doi.org/10.1126/science.aaa1668

Badgley, G., Field, C. B., & Berry, J. A. (2017). Canopy near-infrared reflectance and terrestrial photosynthesis. *Science Advances*, *3*(3), e1602244. https://doi.org/10.1126/sciadv.1602244

Biederman, J. A., Scott, R. L., Bell, T. W., Bowling, D. R., Dore, S., Garatuza-Payan, J., … Goulden, M. L. (2017). Carbon and water exchange across dryland ecosystems of southwestern North America. *Global Change Biology*, *23*(10), 4204–4221. https://doi.org/10.1111/gcb.13686

Biederman, J. A., Scott, R. L., Goulden, M. L., Vargas, R., Litvak, M. E., Kolb, T. E., … Burns, S. P. (2016). Terrestrial carbon balance in a drier world: The effects of water availability in southwestern North America. *Global Change Biology*, *22*(5), 1867–1879. https://doi.org/10.1111/gcb.13222

Coops, N. C., Hilker, T., Hall, F. G., Nichol, C. J., & Drolet, G. G. (2010). Estimation of light-use efficiency of terrestrial ecosystems from space: A status report. *Bioscience*, *60*(10), 788–797. https://doi.org/10.1525/bio.2010.60.10.5

Duveiller, G., & Cescatti, A. (2016). Spatially downscaling Sun-induced chlorophyll fluorescence leads to an improved temporal correlation with gross primary productivity. *Remote Sensing of Environment*, *182*, 72–89.

Frankenberg, C., Fisher, J. B., Worden, J., Badgley, G., Saatchi, S. S., Lee, J.-E., … Yokota, T. (2011). New global observations of the terrestrial carbon cycle from GOSAT: Patterns of plant fluorescence with gross primary productivity. *Geophysical Research Letters*, *38*, L17706. https://doi.org/10.1029/2011GL048738

Gamon, J. A., Huemmrich, K. F., Wong, C. Y. S., Ensminger, I., Garrity, S., Hollinger, D. Y., … Peñuelas, J. (2016). A remotely sensed pigment index reveals photosynthetic phenology in evergreen conifers. *Proceedings of the National Academy of Sciences of the United States of America*, *113*(46), 13,087–13,092. https://doi.org/10.1073/pnas.1606162113

Gamon, J. A., Peñuelas, J., & Field, C. B. (1992). A narrow-waveband spectral index that tracks diurnal changes in photosynthetic efficiency. *Remote Sensing of Environment*, *41*(1), 35–44. https://doi.org/10.1016/0034-4257(92)90059-S

Guanter, L., Aben, I., Tol, P., Krijger, J. M., Hollstein, A., Köhler, P., … Landgraf, J. (2015). Potential of the TROPOspheric Monitoring Instrument (TROPOMI) onboard the Sentinel-5 Precursor for the monitoring of terrestrial chlorophyll fluorescence. *Atmospheric Measurement Techniques*, *8*(3), 1337–1352. https://doi.org/10.5194/amt-8-1337-2015

He, M., Kimball, J. S., Running, S., Ballantyne, A., Guan, K., & Huemmrich, F. (2016). Satellite detection of soilmoisture related water stress impacts on ecosystem productivity using the MODIS-based photochemical reflectance index. *Remote Sensing of Environment*, *186*, 173–183. https://doi.org/10.1016/j.rse.2016.08.019

Jeong, S. J., Schimel, D., Frankenberg, C., Drewry, D. T., Fisher, J. B., Verma, M., … Joiner, J. (2017). Application of satellite solar-induced chlorophyll fluorescence to understanding large-scale variations in vegetation phenology and function over northern high latitude forests. *Remote Sensing of Environment*, *190*, 178–187. https://doi.org/10.1016/j.rse.2016.11.021

Joiner, J., Guanter, L., Lindstrot, R., Voigt, M., Vasilkov, A. P., Middleton, E. M., … Frankenberg, C. (2013). Global monitoring of terrestrial chlorophyll fluorescence from moderate spectral resolution near-infrared satellite measurements: Methodology, simulations, and application to GOME-2. *Atmospheric Measurement Techniques Discussions*, *6*(2), 3883–3930. https://doi.org/10.5194/amtd-6-3883-2013

Joiner, J., Yoshida, Y., Guanter, L., & Middleton, E. M. (2016). New methods for the retrieval of chlorophyll red fluorescence from hyperspectral satellite instruments: Simulations and application to GOME-2 and SCIAMACHY. *Atmospheric Measurement Techniques*, *9*(8), 3939–3967. https://doi.org/10.5194/amt-9-3939-2016

Jones, L. A., Kimball, J. S., Reichle, R. H., Madani, N., Glassy, J., Ardizzone, J. V., … Scott, R. L. (2017). The SMAP level 4 carbon product for monitoring ecosystem land-atmosphere CO_2 exchange. *IEEE Transactions on Geoscience and Remote Sensing*, *55*(11), 6517–6532. https://doi.org/10.1109/TGRS.2017.2729343

Jung, M., Reichstein, M., Margolis, H. A., Cescatti, A., Richardson, A. D., Arain, M. A., … Williams, C. (2011). Global patterns of land-atmosphere fluxes of carbon dioxide, latent heat, and sensible heat derived from eddy covariance, satellite, and meteorological observations. *Journal of Geophysical Research*, *116*, G00J07. https://doi.org/10.1029/2010JG001566

Jung, M., Reichstein, M., Schwalm, C. R., Huntingford, C., Sitch, S., Ahlström, A., … Zeng, N. (2017). Compensatory water effects link yearly global land CO_2 sink changes to temperature. *Nature*, *541*(7638), 516–520. https://doi.org/10.1038/nature20780

Keeling, C., Whorf, T., Wahlen, M., & Plicht, J. (1995). Interannual extremes in the rate of rise of atmospheric carbon dioxide since 1980. *Nature*, *375*(6533), 666–670. https://doi.org/10.1038/375666a0

Lee, J., Berry, J. A., van der Tol, C., Yang, X., Guanter, L., Damm, A., … Frankenberg, C. (2015). Simulations of chlorophyll fluorescence incorporated into the Community Land Model version 4. *Global Change Biology*, *21*(9), 3469–3477. https://doi.org/10.1111/gcb.12948

Lee, J., Frankenberg, C., van der Tol, C., Berry, J. A., Guanter, L., Boyce, C. K., … Saatchi, S. (2013). Forest productivity and water stress in Amazonia: Observations from GOSAT chlorophyll fluorescence. *Proceedings of the Royal Society B*, *280*(1761), 20130171. https://doi.org/10.1098/rspb.2013.0171

Ma, X., Huete, A., Cleverly, J., Eamus, D., Chevallier, F., Joiner, J., … Ponce-Campos, G. (2016). Drought rapidly diminishes the large net CO 2 uptake in 2011 over semi-arid Australia Jiangsu Center for Collaborative Innovation in Geographical Information Resource Development and Application. *Scientific Reports*, *6*(1), 37747. https://doi.org/10.1038/srep37747

Ma, X., Huete, A., Moran, S., Ponce-Campos, G., & Eamus, D. (2015). Abrupt shifts in phenology and vegetation productivity under climate extremes. *Journal of Geophysical Research: Biogeosciences*, *120*, 2036–2052. https://doi.org/10.1002/2015JG003144

Ma, X., Huete, A., Yu, Q., Restrepo-Coupe, N., Beringer, J., Hutley, L. B., … Eamus, D. (2014). Parameterization of an ecosystem light-use-efficiency model for predicting savanna GPP using MODIS EVI. *Remote Sensing of Environment*, *154*, 253–271. https://doi.org/10.1016/j.rse.2014.08.025

Monteith, J. (1972). Solar radiation and productivity in tropical ecosystems. *Journal of Applied Ecology*, *9*(3), 747–766. https://doi.org/10.2307/2401901

Parazoo, N. C., Bowman, K., Fisher, J. B., Frankenberg, C., Jones, D. B. A., Cescatti, A., … Montagnani, L. (2014). Terrestrial gross primary production inferred from satellite fluorescence and vegetation models. *Global Change Biology*, *20*(10), 3103–3121. https://doi.org/10.1111/gcb.12652

Penuelas, J., Garbulsky, M. F., & Filella, I. (2011). Photochemical reflectance index (PRI) and remote sensing of plant CO_2 uptake. *New Phytologist*, *191*(3), 596–599. https://doi.org/10.1111/j.1469-8137.2011.03791.x

Perez-Priego, O., Guan, J., Rossini, M., Fava, F., Wutzler, T., Moreno, G., … Migliavacca, M. (2015). Sun-induced chlorophyll fluorescence and photochemical reflectance index improve remote-sensing gross primary production estimates under varying nutrient availability in a typical Mediterranean savanna ecosystem. *Biogeosciences*, *12*(21), 6351–6367. https://doi.org/10.5194/bg-12-6351-2015

Porcar-Castell, A., Tyystjärvi, E., Atherton, J., Van Der Tol, C., Flexas, J., Pfündel, E. E., … Berry, J. A. (2014). Linking chlorophyll a fluorescence to photosynthesis for remote sensing applications: Mechanisms and challenges. *Journal of Experimental Botany*, *65*(15), 4065–4095. https://doi.org/10.1093/jxb/eru191

Potter, C., Randerson, J., & Field, C. (1993). Terrestrial ecosystem production: A process model based on global satellite and surface data. *Global Biogeochemical Cycles*, *7*(4), 811–841. https://doi.org/10.1029/93GB02725

Poulter, B., Frank, D., Ciais, P., Myneni, R. B., Andela, N., Bi, J., … van der Werf, G. R. (2014). Contribution of semi-arid ecosystems to interannual variability of the global carbon cycle. *Nature*, *509*(7502), 600–603. https://doi.org/10.1038/nature13376

Running, S. W., Nemani, R. R., Heinsch, F. A., Zhao, M., Reeves, M., & Hashimoto, H. (2004). A continuous satellite-derived measure of global terrestrial primary production. *Bioscience*, *54*(6), 547–560. https://doi.org/10.1641/0006-3568(2004)054%5B0547:ACSMOG%5D2.0.CO;2

Sanders, A. F. J., Verstraeten, W. W., Kooreman, M. L., van Leth, T. C., Beringer, J., & Joiner, J. (2016). Spaceborne Sun-induced vegetation fluorescence time series from 2007 to 2015 evaluated with Australian fluxtower measurements. *Remote Sensing*, *8*(12), 895. https://doi.org/10.3390/rs8110895

Schimel, D., Pavlick, R., Fisher, J. B., Asner, G. P., Saatchi, S., Townsend, P., … Cox, P. (2015). Observing terrestrial ecosystems and the carbon cycle from space. *Global Change Biology*, *21*(5), 1762–1776. https://doi.org/10.1111/gcb.12822

Scott, R. L., Biederman, J. A., Hamerlynck, E. P., & Barron-Gafford, G. A. (2015). The carbon balance pivot point of southwestern U.S. semiarid ecosystems: Insights from the 21st century drought. *Journal of Geophysical Research: Biogeosciences*, *120*, 2612–2624. https://doi.org/10.1002/2015JG003181

Scott, R. L., Jenerette, G. D., Potts, D. L., & Huxman, T. E. (2009). Effects of seasonal drought on net carbon dioxide exchange from a woody-plant-encroached semiarid grassland. *Journal of Geophysical Research*, *114*, G04004. https://doi.org/10.1029/2008JG000900

Sims, D. A., Brzostek, E. R., Rahman, A. F., Dragoni, D., & Phillips, R. P. (2014). An improved approach for remotely sensing water stress impacts on forest C uptake. *Global Change Biology*, *20*(9), 2856–2866. https://doi.org/10.1111/gcb.12537

Sims, D. A., Rahman, A. F., Cordova, V. D., El-Masri, B. Z., Baldocchi, D. D., Bolstad, P. V., … Xu, L. (2008). A new model of gross primary productivity for North American ecosystems based solely on the enhanced vegetation index and land surface temperature from MODIS. *Remote Sensing of Environment*, *112*(4), 1633–1646. https://doi.org/10.1016/j.rse.2007.08.004

Smith, W. K., Reed, S. C., Cleveland, C. C., Ballantyne, A. P., Anderegg, W. R. L., Wieder, W. R., … Running, S. W. (2016). Large divergence of satellite and Earth system model estimates of global terrestrial CO_2 fertilization. *Nature Climate Change*, *6*(3), 306–310. https://doi.org/10.1038/nclimate2879

Stavros, E. N., Schimel, D., Pavlick, R., Serbin, S., Swann, A., Duncanson, L., … Wennberg, P. (2017). ISS observations offer insights into plant function. *Nature Ecology and Evolution*, *1*, 0194.

Sun, Y., Frankenberg, C., Wood, J. D., Schimel, D. S., Jung, M., Guanter, L., … Yuen, K. (2017). OCO-2 advances photosynthesis observation from space via solar-induced chlorophyll fluorescence. *Science*, *358*, eaam5747

Verma, M., Friedl, M. A., Richardson, A. D., Kiely, G., Cescatti, A., Law, B. E., … Propastin, P. (2014). Remote sensing of annual terrestrial gross primary productivity from MODIS: An assessment using the FLUXNET la Thuile data set. *Biogeosciences*, *11*(8), 2185–2200. https://doi.org/10.5194/bg-11-2185-2014

Verma, M., Schimel, D., Evans, B., Frankenberg, C., Beringer, J., Drewry, D., … Eldering, A. (2017). Effect of environmental conditions on the relationship amongst OCO-2 SIF, MODIS PRI, and tower GPP at an OzFlux grassland site. *Journal of Geophysical Research: Biogeosciences*, *122*, 716–733. https://doi.org/10.1002/2016JG003580

Vicca, S., Balzarolo, M., Filella, I., Granier, A., Herbst, M., Knohl, A., … Peñuelas, J. (2016). Detection of effects of extreme droughts on gross primary production using satellite data. *Scientific Reports*, *6*(1), 28269. https://doi.org/10.1038/srep28269

Walther, S., Voigt, M., Thum, T., Gonsamo, A., Zhang, Y., Kohler, P., … Guanter, L. (2016). Satellite chlorophyll fluorescence measurements reveal large-scale decoupling of photosynthesis and greenness dynamics in boreal evergreen forests. *Global Change Biology*, *22*(9), 2979–2996. https://doi.org/10.1111/gcb.13200

Wood, J. D., Griffis, T. J., Baker, J. M., Frankenberg, C., Verma, M., & Yuen, K. (2016). Multiscale analyses of solar-induced florescence and gross primary production. *Geophysical Research Letters*, *44*, 533–541. https://doi.org/10.1002/2016GL070775

Xiao, J., Ollinger, S. V., Frolking, S., Hurtt, G. C., Hollinger, D. Y., Davis, K. J., … Suyker, A. E. (2014). Data-driven diagnostics of terrestrial carbon dynamics over North America. *Agricultural and Forest Meteorology*, *197*, 142–157. https://doi.org/10.1016/j.agrformet.2014.06.013

Yang, H., Yang, X., Zhang, Y., Heskel, M. A., Lu, X., Munger, J. W., … Tang, J. (2017). Chlorophyll fluorescence tracks seasonal variations of photosynthesis from leaf to canopy in a temperate forest. *Global Change Biology*, *23*(7), 2874–2886. https://doi.org/10.1111/gcb.13590

Yang, X., Tang, J., Mustard, J. F., Lee, J., & Rossini, M. (2015). Solar-induced chlorophyll fluorescence correlates with canopy photosynthesis on diurnal and seasonal scales in a temperate deciduous forest. *Geophysical Research Letters*, *42*, 2977–2987. https://doi.org/10.1002/2015GL063201

Zarco-Tejada, P. J., González-Dugo, M. V., & Fereres, E. (2016). Seasonal stability of chlorophyll fluorescence quantified from airborne hyperspectral imagery as an indicator of net photosynthesis in the context of precision agriculture. *Remote Sensing of Environment*, *179*, 89–103. https://doi.org/10.1016/j.rse.2016.03.024

Zhang, Y., Guanter, L., Berry, J. A., Joiner, J., van der Tol, C., Huete, A., … Köhler, P. (2014). Estimation of vegetation photosynthetic capacity from space-based measurements of chlorophyll fluorescence for terrestrial biosphere models. *Global Change Biology*, *20*(12), 3727–3742. https://doi.org/10.1111/gcb.12664

Zhao, M., Heinsch, F. A., Nemani, R. R., & Running, S. W. (2005). Improvements of the MODIS terrestrial gross and net primary production global data set. *Remote Sensing of Environment*, *95*(2), 164–176. https://doi.org/10.1016/j.rse.2004.12.011

Zhao, M., & Running, S. W. (2010). Drought-induced reduction in global terrestrial net primary production from 2000 through 2009. *Science*, *1667*, 2–5.